ACS APPLIED MATERIALS & INTERFACES

Research Article

www.acsami.org

Synthesis and Characterization of the Hole-Conducting Silica/Polymer Nanocomposites and Application in Solid-State Dye-Sensitized Solar Cell

Wen Yuan,*[,†] Hui Zhao,[†] Heyi Hu,[†] Shen Wang,[‡] and Gregory L. Baker[†,§]

[†]Department of Chemistry, Michigan State University, East Lansing, Michigan 48824, United States

[‡]Institute of Physics, Chinese Academy of Sciences, Beijing 100190, China

Supporting Information

ABSTRACT: Hole-conducting silica/polymer nanocomposites exhibit interesting physical and chemical properties with important applications in the field of energy storage and hybrid solar cells. Although the conventional strategy of grafting hole-conducting polymer onto the surface of silica nanoparticles is to use in situ oxidative polymerization, a promising alternative of using surface-initiated controlled living radical polymerization has arisen to anchor the polymer on the silica. The resulting silica/polymer nanocomposites from the latter method are more chemically and thermally stable because of the strong covalent bonding compared to the electrostatic interaction from in situ polymerization. The use of these nanocomposites mixed with spiro-MeOTAD (2,2′,7,7′-tetrakis(*N*,*N*-di-*p*-methoxyphenyl-amine)-9,9′-spirobifluorene) as a new hole conductor in the application of solid-state dye-sensitized solar cell (ss-DSSC) is reported here. The power conversion efficiency of this ss-DSSC is higher than the full spiro-MeOTAD ss-DSSC. Notably, the short circuit current improves by 26%. It is explained by large size silica/polymer nanocomposites forming an additional light scattering layer on the top of photoanode. This is the first time a conductive light scattering layer is introduced into ss-DSSC to enhance cell performance.

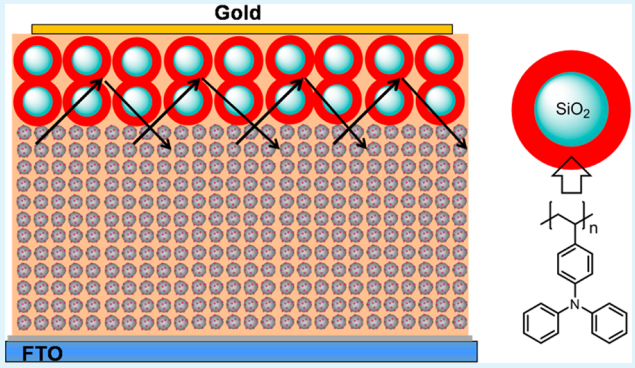

KEYWORDS: *surface-initiated polymerization, silica/polymer nanocomposites, triphenylamine, solid conductors, light-scattering layer, solid-state dye-sensitized solar cell*

1. INTRODUCTION

Increasing attention has been paid in preparation and application of organic/inorganic nanocomposite materials for decades because of the novel chemical and physical properties.[1−4] Here, "organic" means an organic molecular or polymer and "inorganic" includes silica,[2] metal,[5] quantum dots,[6] metal oxide semiconductor,[7] and magnetic nanoparticle.[8] These composite materials are synthesized through physically blending, interfacial interaction, in situ polymerization, or other methods that can offer us different thermal, mechanical properties, and optimized for biomedical and electrical application. Silica nanoparticles have exhibit a good thermal, chemical, and optical stability with well-defined, size-tunable structure. Thus grafting different functional organic layers onto the silica particles has been explored in many areas.[2]

Hole conducting hybrid silica-based nanocomposites[2,9] use silica particles as core structure and hole conducting polymer as shell layer. The conducting shell layer coated on silica includes such as polypyrrole,[10] polyaniline,[11,12] or polythiophene.[13] The conventional grafting strategy is to use in situ oxidative polymerization.[10−13] For instance, polythiophene-coated silica nanocomposite was synthesized from the direct dispersion polymerization of the thiophene monomers using ammonium peroxodisulfate as oxidant.[13] However, this type of grafting strategy is mainly attributable to the noncovalent bonding from electrostatic interactions.[12] Extensively washing or ultrasonication is both able to peel off the polymer layer. On the other hand, grafting polymer from a surface initiator forms the strong covalent bond between substrate surface and polymer shell. To achieve that, one of the most widely used methods is via controlled living radical polymerization (CLRP).[14−21] Among different CLRP methods, nitroxide mediate polymerization (NMP)[20−23] is especially attractive for its fine control over the molecular weight of the grafted polymers, facile polymerization of styrene-like monomer, and the feasibility of metal-free polymerization.

Triphenylamine is one of the most common building blocks for hole conductors. It is widely utilized in the fields such as organic light-emitting diodes,[24] polymer solar cell,[25] and ss-DSSC.[26−29] Recently, a new record efficiency of ss-DSSC with

Received: January 15, 2013
Accepted: April 22, 2013
Published: April 22, 2013

   dx.doi.org/10.1021/am4001858 | ACS Appl. Mater. Interfaces 2013, 5, 4155−4161

Scheme 1. Synthesis of 4-Vinyl-triphenylamine (4VTPA) and Poly-4-vinyl-triphenylamine (P4VTPA)

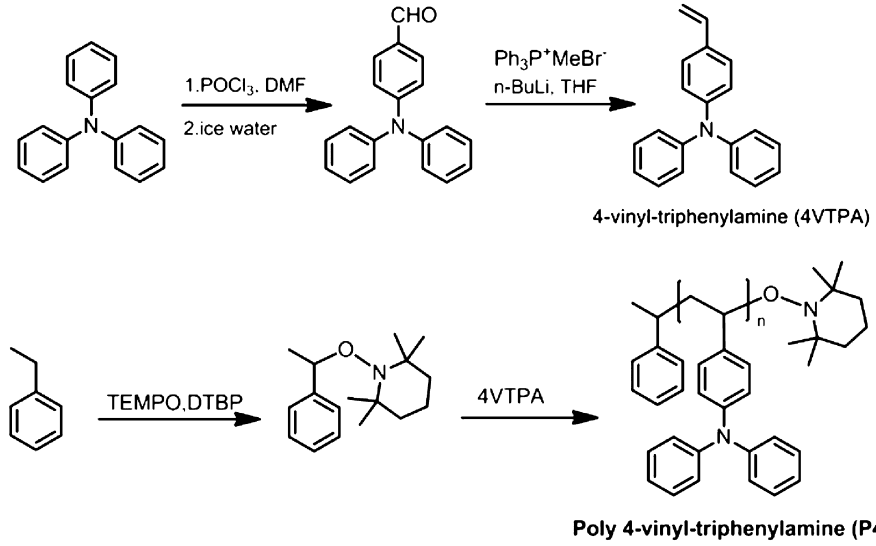

novel hole conductors of greater 10% has been reported,[30,31] which is still below a desired level for practical application. And the high cost of hole conductors and low photocurrent of ss-DSSC have prohibited the advancement of ss-DSSC in the past decade. Spiro-MeOTAD[26,27] (2,2′,7,7′ -tetrakis(*N*,*N*-di-*p*-methoxyphenylamine)-9,9′-spirobifluorene), which contains four triphenylamine units in structure for charge transporting, has been one of the most promising hole conductors hitherto. However, the price of spiro-MeOTAD hardly goes down and few manufacturers are able to provide only lab-scale spiro-MeOTAD. All of these practical situations retard the development of ss-DSSC.

Here we report the synthesis of a thermally stable poly(triphenylamine)-grafted-silica nanoparticle by surface-initiated nitroxide-mediated polymerization (SI-NMP). We apply this conducting silica/polymer nanocomposite on the application of ss-DSSC. By combining silica/polymer nanocomposites with spiro-MeOTAD as hole conductor, the power conversion efficiency of our ss-DSSC improves as a result of enhanced photocurrent. This enhancement in photocurrent comes from an additional light scattering layer formed by silica/polymer nanocomposites. This new composite material has effectively reduced the cost of ss-DSSC by lowering the spiro-MeOTAD loading, while maintaining the cell's performance.

2. EXPERIMENTAL SECTION

2.1. Materials. Aerosil 200 silica nanoparticle was a gift from Degussa. Fluorine doped Tin Oxide (FTO) Glass purchased from Hartford was pretreated by Alconox, distilled water, acetone and UV-ozone before use. Spiro-MeOTAD was purchased from Lumtech. TiO_2 paste (Ti-Nanoxide T) was from Solaronix. Gold used as evaporation source for counter electrode was from Kurt J. Lesker. All other chemicals were purchased from Sigma Aldrich and were used as receive unless mentioned otherwise.

2.2. Instruments. All Fourier transform infrared spectroscopy (FTIR) spectra were acquired from a Mattson Galaxy 300 spectrometer purged with dry nitrogen, with the signal averaging 128 scans. All IR samples were dried, ground and mixed with KBr and then pressed into pellets. Thermogravimetric analyses (TGA) were obtained in air using a Perkin-Elmer TGA 7. The heating rate is 10 °C/min, and samples were held at 120 °C for 30 min before running. Differential scanning calorimetry (DSC) measurements were carried out using a TA DSC Q100 with a heating/cooling rate of 10 °C/min under nitrogen. Absorption spectra were obtained from Varian Carey model 50 UV−vis spectrophotometer. The molecular weights of polymers were determined by gel permeation chromatography (GPC) at 35 °C using two PLgel 10-lm mixed-B columns in series with THF as the eluting solvent. X-ray photoelectron spectroscopy (XPS) analysis was carried out in a Perkin-Elmer Phi 5600 ESCA system with magnesium Ka X-ray source. Dynamic light scattering (DLS) study was carried out on Malvern Zetasizer Nanoseries ZEN3600 instrument at 30 °C. Morphology of silica/polymer film was captured by Veeco Dimension 3100 scanning probe microscope. The cross-sectional structure of solar cell was determined by a Hitachi S-4700 II field-emission scanning electron microscope (FESEM). The samples were soaked in liquid nitrogen before fracturing.

Current−voltage measurements and open circuit voltage decay measurements of ss-DSSC were performed using a Xe Arc Lamp and CHI-650D Electrochemical workstation. A mask with an area of 0.25 cm^2 was used. An AM 1.5 solar filter and neutral density filter were used to simulate sunlight at 100 mW cm^{-2}. A Horiba Jobin Yvon MicroHR was used for monochromatic light.

2.3. Synthesis. Synthesis of poly 4-vinyl-triphenylamine (P4VTPA): The recipe of free polymer followed a procedure of polystyrene by NMP.[22] In our case the monomer, 4-vinyl-triphenylamine and initiator were dissolved in dry, freshly distilled diglyme or toluene and polymerized in a Schlenk flask at 110 °C under nitrogen. After polymerized over 36 h, the polymers were precipitated from acetone first and reprecipitated three times from THF/acetone. A Soxhlet extraction was used for further purification. The free polymer was dried by vacuum under 80 °C at least 6 h before any measurements.

Synthesis of silica/polymer nanocomposites: A surface-initiated NMP of 4-vinyl-triphenylamine here was carried out with silica initiator. The silica initiator and surface-initiated polymerization was prepared according to a literature procedure.[20] To a Schlenk flask equipped with a magnetic stirrer, was added silica initiator, monomer, and distilled toluene as solvent. The mixture was ultrasonicated for 5 min to make particles dispersed well in solvent. After three cycles of freeze−pump−thaw, the Schlenk flask was filled with nitrogen at room temperature and the polymerization started at 110 °C with rapid stirring. The polymerization was stopped after 48 h. Then the silica nanoparticles were extensively washed-centrifuged by toluene and acetone for several times in order to removing the excess monomer and free polymer. The silica/polymer nanocomposites were finally dried by vacuum under 80 °C at least 6 h before any measurements.

2.4. Solar Cell Fabrication and Preparation. Devices of ss-DSSC were fabricated according to a procedure.[29] Briefly, a precleaned FTO glass was put on a hot plate with a temperature of 500 °C for 30

Scheme 2. Synthesis of Silica-P4VTPA Nanocomposite

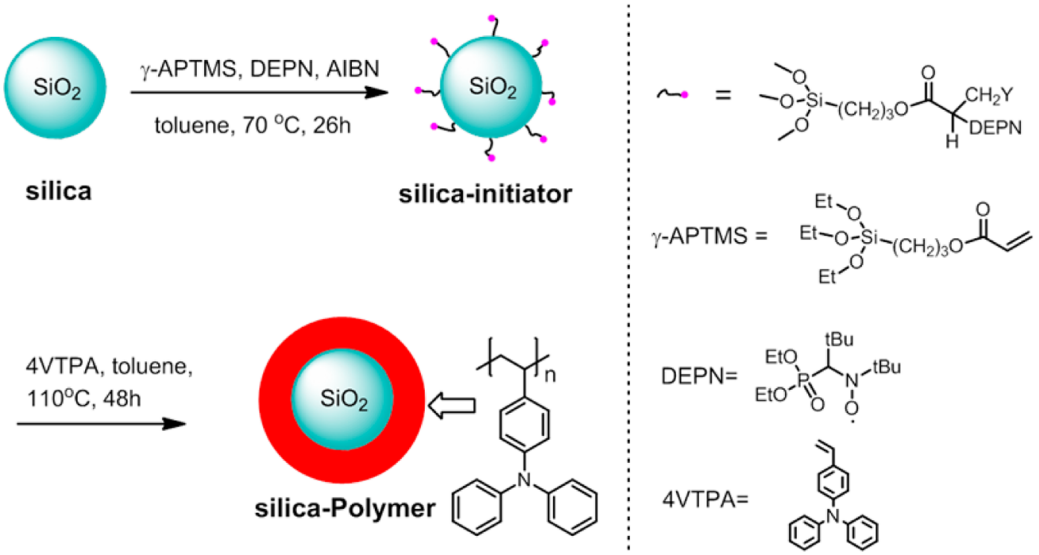

min before any deposition. A 200 nm thickness of TiO_2 compact layer on FTO was formed by homemade spray-pyrolysis setup using air as carrier gas and titanium di-isopropoxide bis (acetylacetonate) as precursor. A 2.5 μm thickness of mesoporous TiO_2 film was deposited by doctor-blading TiO_2 pastes with scotch tape as spacer. The thickness was measured by profilometer and confirmed by cross-section SEM image. After baking the TiO_2 paste with a programmable heating procedure up to 450 °C, we let the substrate cooling down to 80 °C before soaking into an 0.3 mM N3 dye ethanol solution. The dye soaking took about 16 h at least, followed by rinsing with ethanol and acetonitrile. A chlorobenzene solution of spiro-MeOTAD or mixture of spiro-MeOTAD and silica/polymer were used for spin-coating on dye-coated TiO_2 substrates. The concentration of hole conductors was 120 mg/mL in total with additives of lithium bis (trifluoromethylsulfonyl) imide (LiTFSI) solution (26 μL/mL, LiTFSI predissolved in acetonitrile with a concentration of 170 mg/mL) and 4-tert butylpyridine (4-tBP) (12 μL/mL). A 36 μL electrolyte solution first stood on the substrate for one minute and then was spin-coated with 2000 rpm for 30 s in air. The cell was stored under dark overnight before depositing the gold electrode. A 30 nm thickness of gold was applied by thermal evaporation as back contact.

3. RESULTS AND DISCUSSION

3.1. Synthesis and characterization of silica/polymer nanocomposite. The synthetic route of both monomer and free polymer are shown in scheme 1. The monomer, 4-vinyl-triphenylamine (4VTPA) is readily prepared in two steps from a commercial available triphenylamine following a procedure.[32] Vinyl group on triphenylamine is the functional group for polymerization. The free polymer (P4VTPA) has been prepared by NMP using an alkoxyamine derivative as unimolecular initiator according to Hawker's procedure of polystyrene.[22] By GPC analysis the polymer gives a M_n = 11 000 g/mol with a low polydispersity index (PDI) of 1.07 after purification. Later, we will use this free polymer (P4VTPA) as standard helping to confirm the chemical structure and compare thermal properties with silica/polymer nanocomposites. Here the silica/polymer nanocomposites are synthesized by SI-NMP. Using thermal initiator such as azobis (isobutyronitrile) (AIBN) or ditert-butyl peroxide (DTBP) along with nitroxide such as 2,2,6,6-tetramethyl-1-1piperdinyloxy (TEMPO) or its alkoxyamine derivative has initiated and controlled the polymerization well. However, the reaction proceeds slowly because of low polymerization rate, especially in the condition of surface-initiated polymerization. The equilibrium constant of phosphonylated nitroxide-based polymerization is much larger than a polymerization using TEMPO as initiator,[33] which allows the polymerization rate based on phosphonylated nitroxide is much larger than on TEMPO. Previous reports from Bartholome and co-workers[20,34] have used N-tert-butyl-N-[1-diethylphosphono(2,2-dimethylpropy)] nitroxide (DEPN) as surface initiator to grow styrene on silica nanoparticles successfully. We optimize this procedure and use 4VTPA instead of styrene in the literature. Scheme 2 presents a detail of this surface-initiated polymerization in two steps: (1) in situ attaching acrylic phosphonylated alkoxyamine on the surface of silica, and (2) growing triphenylamine polymer from silica nanoparticles.

Figure 1 shows the FTIR spectra of materials at different stages. The IR spectrum of bared silica displays a broad peak in

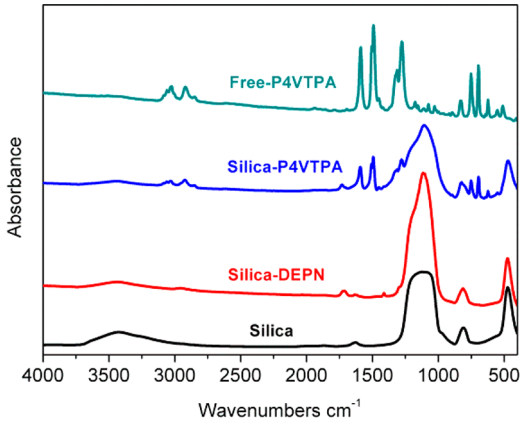

Figure 1. FTIR spectra of bared silica, silica-DEPN, silica-P4VTPA, and free-P4VTPA (from bottom to top).

the range of 3000−3600 cm^{-1}, which indicates the O−H stretching. This hydroxyl signal is due to the silanol group and the physisorbed moisture on silica. Additionally, the peaks centered at 790 and 1150 cm^{-1} represent the Si−O stretching. After the immobilization of initiator (Silica-DEPN), peaks of

dx.doi.org/10.1021/am4001858 | ACS Appl. Mater. Interfaces 2013, 5, 4155−4161

carbonyl ($\nu_{C=O}$, 1750 cm^{-1}) and aliphatic group (ν_{C-H}, 2900 cm^{-1} and δ_{C-H}, 1360 cm^{-1}) appeared. Meanwhile, the absorbance of hydroxyl group from silica decreases due to consuming of silanol group. The structure of silica-DEPN can also be demonstrated by XPS analysis in the Supporting Information (Figure S1 and S2). The IR spectrum of silica/polymer composites (Silica-P4VTPA) shows sp^2 and sp^3 C−H signals attributed from polymer chain and backbone at 3050 and 2800 cm^{-1}. In addition, bands around 1600, 1500 (C−C in aromatic ring), 800, 750, and 700 cm^{-1} (substituted pattern of benzene ring) are consistent with the polymer structure grafting on the silica. An IR spectrum of free P4VTPA in Figure 1 is used as reference here. These data confirm successful grafting of the P4VTPA from silica nanoparticles.

The bared silica nanoparticles used in our research have a particle size of 8−12 nm initially. After initiator's immobilization and surface polymerization, the silica/polymer nanocomposites precipitate out from solution with multiple times washing and centrifugation, followed by drying under vacuum. A DLS result of silica/polymer nanocomposites in diluted solution gives a particle size of 300 nm in diameter due to the particle aggregation.

3.2. Thermal Stability of Silica/Polymer Nanocomposite. Figure 2 shows the thermal degradation measured by

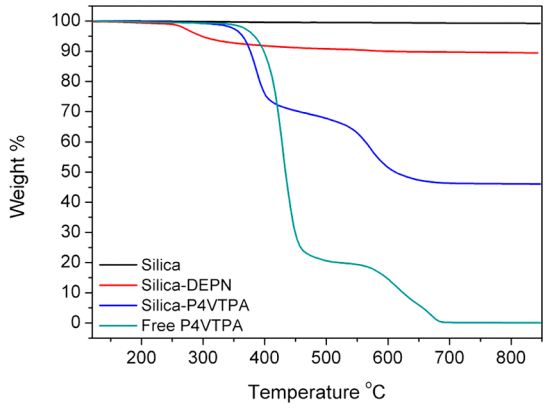

Figure 2. TGA curves for bared silica, silica-DEPN, silica-P4VTPA, and free-P4VTPA.

TGA analyzer. The thermal behavior is observed in the range from 120 to 850 °C under air and all the organic parts will be burnt to gas phase with only silica left. Compared to bared silica nanoparticles, silica-DEPN decomposes at 250 °C with a weight loss of 11% from initiator. After growth of polymer on silica, a better thermal stability can be seen. Decomposition of polymer/silica nanocomposites appears at 350 °C, and finally leads to a 55% weight loss with two-step degradation. The first step is possibly for the loss of side chain of polymers, followed by the second step indicating the combustion of backbone in polymers. The TGA curve of free polymer is also used here in Figure 2 as reference for this conclusion.

Figure 3 displays both the differential scanning calorimetry (DSC) results of free-P4VTPA and silica-P4VTPA. It clearly reveals that glass transition temperature (T_g) of silica/polymer composites gives a value of 152 °C without any crystallization, which is 20 degrees larger than a free polymer. Anchoring polymer on silica nanoparticles should present larger T_g than the free polymer, because the polymer chain would be restricted of movement by silica nanoparticles.[35] Both TGA

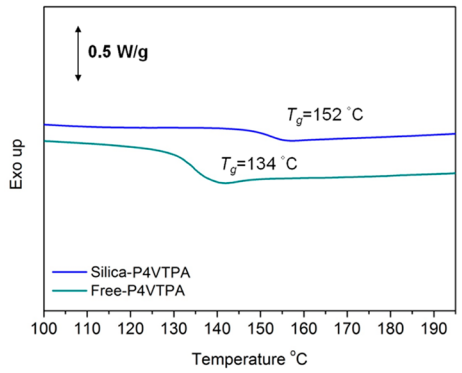

Figure 3. DSC curves of free polymer and silica/polymer nanocomposites.

and DSC results confirm the excellent thermal stability of our silica/polymer nanocomposite, and it is suitable for solar cell's fabrication and operation.

3.3. Cell Performance. Previous reports have already investigated that the incomplete pore filling of hole conductor into mesoporous TiO_2 is what has decelerated dye regeneration in ss-DSSC.[29,36] To achieve a complete infiltration of hole conductor, a small size of hole conductor is necessary to introduce into porous TiO_2. Herein we combine the spiro-MeOTAD together with our hole conducting silica/polymer nanocomposites and then apply them in ss-DSSC. Figure 4

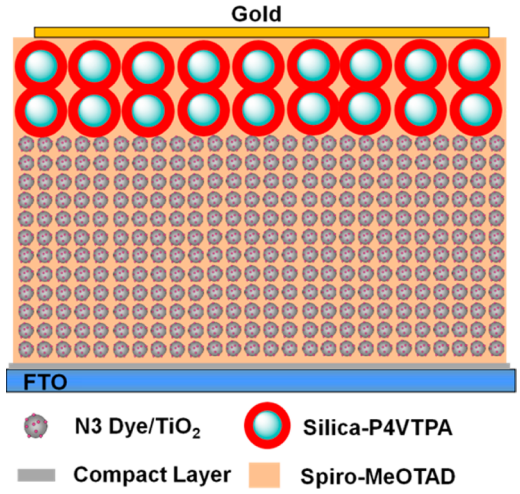

Figure 4. Illustration of ss-DSSC with a capping layer made by silica-P4VTPA.

illustrates a device fabricated basing on hole conductor mixture. A chlorobenzene solution of hole conductor mixture is applied on dye-coated TiO_2 by spin-coating. As seen in Figure 4, the spiro-MeOTAD with smaller size penetrates all through the porous TiO_2, and hole conducting silica/polymer nanocomposites with bigger size will be left on top of TiO_2 forming a capping layer. This capping layer can act as the role of both charge transporting and light scattering. This assumption is further confirmed by the cross-section SEM image (Figure 5). Good penetration and pore-filling can be seen. Silica/polymer nanocomposites with extra spiro-MeOTAD lies on TiO_2 thin layer with a thickness around 2 μm. Previous results suggested the capping layer thickness ranging from 100 to 400 nm would give the optimized performance. Photocurrent and fill factor

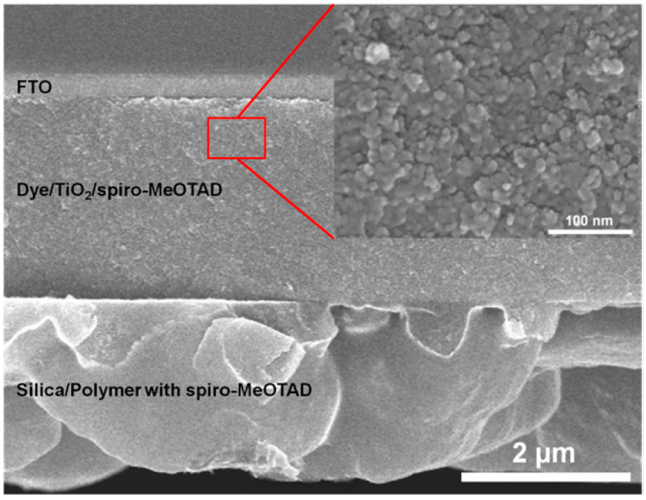

Figure 5. SEM image of cross-sectional structure of ss-DSSC (Inset: information of spiro-MeOTAD filled with TiO_2 pore).

increased in ss-DSSC while thickness decreased, which controlled by hole conductor concentration and spin-coating rate.[36,37] Thicker capping layer would result a higher internal resistance and affect the cell performance. In our system, a 2 μm is not the best condition for fabricating cell. The study of capping layer's thickness and better deposition method are still in optimization, and will be explored in ongoing research.

We fabricate ss-DSSC following a procedure.[29,38] Here, the light absorber used is N3 ruthenium dye, which is the most widely applied light absorber in DSSC. A photoanode is made by sintering a TiO_2 paste (Ti-Nanoxide T) from Solaronix. A spiro-MeOTAD or a mixture of spiro-MeOTAD and silica/polymer nanocomposites is used as hole conductor in ss-DSSC. A 30 nm thickness of gold as counter electrode applies on the very top of cell in Figure 4. Three different types of devices are made and characterized for comparison (Figure 6). One is a full

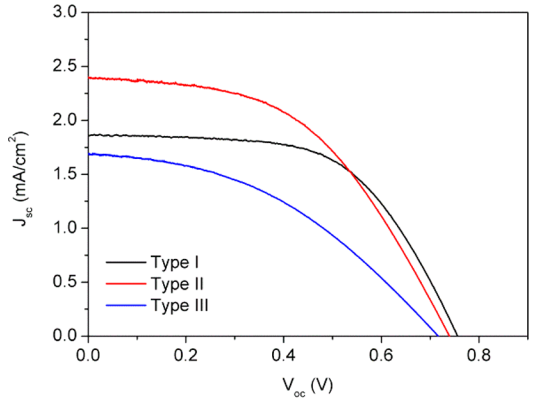

Figure 6. $J-V$ curves of ss-DSSC with different types of hole conductors.

spiro-MeOTAD-based ss-DSSC (Type I). Another two ss-DSSCs, type II and type III, are a mixture of spiro-MeOTAD and nanocomposites as hole conductor in two different weight ratios, 1:1 or 3:1, respectively. Additionally, we mix the spiro-MeOTAD with bared silica nanoparticles as the control, but silica particles cannot disperse well in chlorobenzene without any polymer layer grafting on its surface. This may be due to the hydrophobic−hydrophobic interaction between solvent and polymer layer. We've changed DMF instead of chlorobenzene as solvent and fabricated the ss-DSSC as well. However, a negligible efficiency is observed (see Figure S3 in the Supporting Information). We assumed some of the small silica particles went into TiO_2 pores and retarded spiro-MeOTAD's penetration.

A full spiro-MeOTAD based ss-DSSC fabricated in our lab gives a power conversation efficiency of 0.84%, which is below a standard level above 3%. This is limited by the dye and TiO_2 paste chosen compared to previous procedure.[29] After introducing silica/polymer with spiro-MeOTAD as hole conductor, it enables us to decrease the loading of spiro-MeOTAD. The cost of solar cell is largely saved. When the weight ratio of mixture is 1:1, the short circuit current density (J_{sc}) improves by 26% from 1.9 to 2.6 mA/cm^2. Meanwhile, the fill factor (FF) decreases 15% and open circuit voltage (V_{oc}) lowers slightly compared to a full spiro-MeOTAD-based ss-DSSC (Table 1). The overall efficiency of the type II cell

Table 1. Summary of Three Types of Solar Cells' Performance

	silica-P4VTPA (%)[a]	J_{sc} (mA/cm^2)	V_{oc} (V)	FF	η (%)
type I	0	1.9	0.76	0.58	0.84
type II	50	2.4	0.74	0.49	0.87
type III	25	1.7	0.72	0.41	0.50

[a]: weight percentage of silica-P4VTPA in hole conductor mixture.

increases a little bit eventually compared with the device made of all spiro-MeOTAD. The reason for the lower FF from the type II cell is because of the low hole mobility of capping layer with a thicker capping layer. The hole mobility of free polymer P4VTPA is 3.1×10^{-6} cm^2/(V s),[39] which is 10 times less than spiro-MeOTAD.[40] Additionally, the highest occupied molecular orbital (HOMO) level of P4VTPA is 0.2 eV lower than spiro-MeOTAD,[39] which may also affect the charge transporting. And we assume that silica particles do not have any benefit effect to carrier mobility after grafting P4VTPA on silica. Thus, a resulted internal resistance should bring a lower FF and low J_{sc} into device. Similarly, we can also explain of both poorer FF and J_{sc} from type III cell.

However, the photocurrent significantly increases at short circuit from type II cell while adding silica/polymer composites. We think the higher current is because of extra light scattering applied from the capping layer. From the AFM image of the capping layer in Figure 7, we can see apparently silica/polymer nanocomposites as capping layer lying on dye-coated TiO_2. The particles of a size around 250−350 nm aggregate well with a local roughness of 8.1 nm. The size of silica/polymer nanocomposites from AFM confirms our DLS results as well. Morphology of dye-coated TiO_2 has also been imaged by AFM in Supporting Information (Figure S4). Before forming capping layer, a dye-coated TiO_2 shows a size of particle in the range of 15−20 nm. To the best of our knowledge, this is the first time people have tried to introduce hole-conductive light scattering layer into ss-DSSC.

To prove our hypothesis of light scattering effect, we measure the absorbance of different types of devices by using the UV−vis spectroscopy. Figure 8 shows the UV−vis absorbance of three types of ss-DSSC from Table 1 without counter electrode. A cell with only dye-coated TiO_2 on FTO glass is also shown here. In Figure 8, N3 dye-coated-TiO_2 absorbs the light at 535 nm. By spin-coating only spiro-

dx.doi.org/10.1021/am4001858 | ACS Appl. Mater. Interfaces 2013, 5, 4155−4161

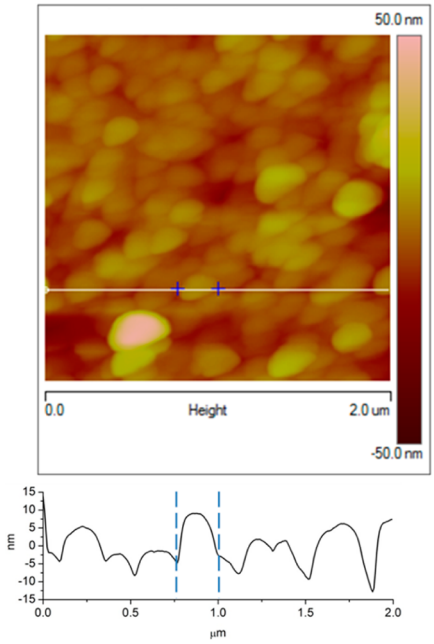

Figure 7. AFM image of silica/polymer nanocomposites as light-scattering layer in ss-DSSC and corresponding linear cross-section profiles analysis.

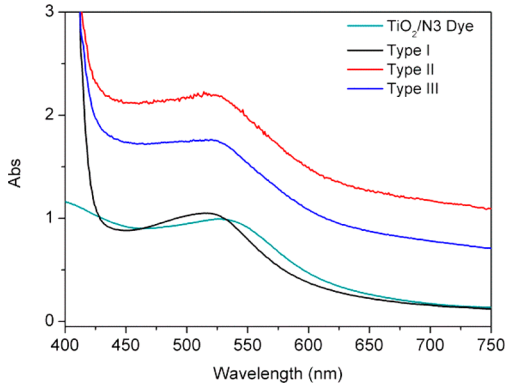

Figure 8. Absorption spectra of N3 dye-coated TiO_2 on FTO and three types of solar cell without gold electrode.

MeOTAD on it, a strong UV absorption occurs from 425 nm from triphenylamine units in spiro-MeOTAD. Because the spiro-MeOTAD film is transparent in the visible-light region, it is hardly to see additional absorption peaks after 425 nm. A small blue shift of the original peak to 520 nm is observed because of the formation of spiro-MeOTAD radical cation under air.[41] Consistently, type II cell and type III cells also absorb green light by N3 dyes. The absorbance remarkably enhances in the range from visible to near IR, because of the light scattering by the capping layer comprising larger-sized nanoparticles. Compared with the type III cell, the type II cell shows a better absorbance because of higher loading of silica/polymer nanocomposites. Figure 9 shows the incident photon-to-current conversion efficiency (IPCE) spectra of three types of ss-DSSC. In the spectra region from 450 to 550 nm, the type II cell exhibits higher IPCE values than type I and type III. Moreover, in the spectral region at near IR region (>650 nm), slight improvement from type II cell can also be seen at 660 and 700 nm. Thus it concludes that photocurrent generated

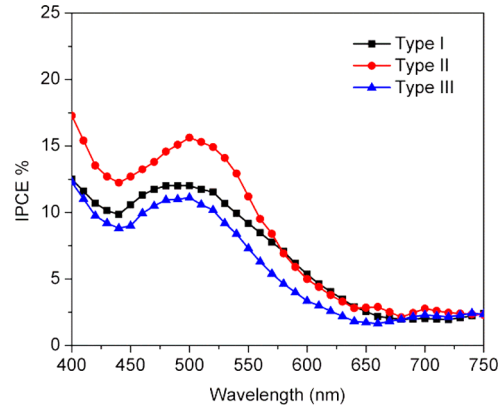

Figure 9. IPCE spectra of and three types of ss-DSSC.

from type II is larger than type I and type III. This is consistent with our results from absorption spectra and Table 1.

Open-circuit voltage decay (OCVD) measurement can provide the information of charge recombination and electron lifetime in DSSC.[42] The potentiostat is used to monitor the decay of V_{oc} after interrupting the constant illumination. The decay of the V_{oc} reveals the decrease in the electron density in DSSC, which is mainly caused by charge recombination. The electron lifetime (τ) is determined by the reciprocal of the derivative of the decay curves normalized by the voltage. In general, longer electron lifetime relates to less charge recombination in DSSC.[42] In Figure 10, the τ versus V_{oc} is

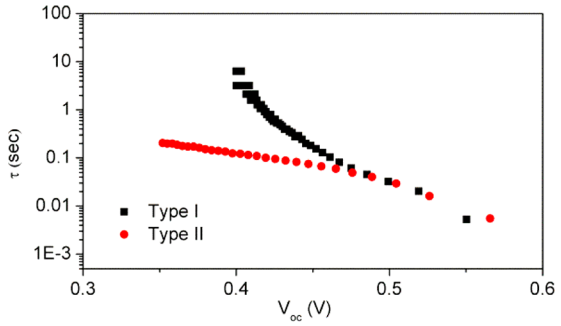

Figure 10. Electron lifetime(τ) derived from corresponding OCVD measurements as a function of V_{oc}.

plotted for type I and type II cells. At a given V_{oc}, especially below 480 mV, the results suggests faster charge recombination from TiO_2 to hole conductor in type II than in type I. As we know in DSSC, V_{oc} loss is due to charge recombination.[43,44] It also concludes V_{oc} in type I cell is 20 mV larger than in type II cell (Figure 6) because of charge recombination.

4. CONCLUSIONS

In conclusion, we first reported grafting poly(triphenylamine) on the surface of silica nanoparticles via surface-initiated nitroxide mediated polymerization (SI-NMP). We combined this thermal stable hole-conducting silica/polymer nanocomposite with spiro-MeOTAD to be applied in ss-DSSC. With only a half of the regular amount of spiro-MeOTAD, the power conversion efficiency of our ss-DSSC was higher than a full spiro-MeOTAD-based ss-DSSC with a 26% improvement in photocurrent. This was due to a light-scattering layer formed by silica/polymer composites on the top of the photoanode which improved the collection of photocurrent. Unfortunately,

the cell's efficiency was still limited by the poor conductivity of silica/polymer composites, which resulted in a poor FF in current−voltage curves. Our ongoing research will focus on functionalizing triphenylamine with different groups to adjust the HOMO level, which will align the energy level of different components in the solar cell and make the charge transport more efficient.

■ ASSOCIATED CONTENT

Supporting Information

XPS data, $J-V$ curve with only bared silica, and AFM image of TiO_2 film. This material is available free of charge via the Internet at http://pubs.acs.org.

■ AUTHOR INFORMATION

Corresponding Author

*Tel: 1-517-355-9715. E-mail: yuanwen@chemistry.msu.edu or yaji861112@gmail.com.

Notes

The authors declare no competing financial interest.

[§]Prof. Gregory L. Baker passed away on Oct. 18. 2012.

■ ACKNOWLEDGMENTS

This work is financially supported by the National Science Foundation (DMR-0934568) and MSU Center for Alternative Energy Storage Research and Technology (CAESRT). W.Y. thanks Dr. James McCusker, Dr. Keith Promislow, and Dr. Lawrence Drzal for valuable discussion.

■ REFERENCES

(1) Sanchez, C.; Julian, B.; Belleville, P.; Popall, M. *J. Mater. Chem.* **2005**, *15*, 3559−3592.
(2) Zou, H.; Wu, S. S.; Shen, J. *Chem. Rev.* **2008**, *108*, 3893−3957.
(3) Sanchez, C.; Belleville, P.; Popall, M.; Nicole, L. *Chem. Soc. Rev.* **2011**, *40*, 696−753.
(4) Chaudhuri, R. G.; Paria, S. *Chem. Rev.* **2012**, *112*, 2373−2433.
(5) Mandal, T. K.; Fleming, M. S.; Walt, D. R. *Nano Lett.* **2002**, *2*, 3−7.
(6) Weaver, J.; Zakeri, R.; Aouadi, S.; Kohli, P. *J. Mater. Chem.* **2009**, *19*, 3198−3206.
(7) Nussbaumer, R. J.; Caseri, W. R.; Smith, P.; Tervoort, T. *Macromol. Mater. Eng.* **2003**, *288*, 44−49.
(8) Burke, N. A. D.; Stover, H. D. H.; Dawson, F. P. *Chem. Mater.* **2002**, *14*, 4752−4761.
(9) Gangopadhyay, R.; De, A. *Chem. Mater.* **2000**, *12*, 608−622.
(10) McCarthy, G. P.; Armes, S. P.; Greaves, S. J.; Watts, J. F. *Langmuir* **1997**, *13*, 3686−3692.
(11) Gill, M.; Armes, S. P.; Fairhurst, D.; Emmett, S. N.; Idzorek, G.; Pigott, T. *Langmuir* **1992**, *8*, 2178−2182.
(12) Jang, J. S.; Ja, J.; Lim, B. *Chem Commun* **2006**, 1622−1624.
(13) Han, M. G.; Armes, S. P. *Langmuir* **2003**, *19*, 4523−4526.
(14) Kim, J. B.; Bruening, M. L.; Baker, G. L. *J. Am. Chem. Soc.* **2000**, *122*, 7616−7617.
(15) Kim, J. B.; Huang, W. X.; Bruening, M. L.; Baker, G. L. *Macromolecules* **2002**, *35*, 5410−5416.
(16) Bao, Z. Y.; Bruening, M. L.; Baker, G. L. *Macromolecules* **2006**, *39*, 5251−5258.
(17) Bao, Z. Y.; Bruening, M. L.; Baker, G. L. *J. Am. Chem. Soc.* **2006**, *128*, 9056−9060.
(18) Pyun, J.; Jia, S. J.; Kowalewski, T.; Patterson, G. D.; Matyjaszewski, K. *Macromolecules* **2003**, *36*, 5094−5104.
(19) Bombalski, L.; Min, K.; Dong, H. C.; Tang, C. B.; Matyjaszewski, K. *Macromolecules* **2007**, *40*, 7429−7432.
(20) Bartholome, C.; Beyou, E.; Bourgeat-Lami, E.; Chaumont, P.; Lefebvre, F.; Zydowicz, N. *Macromolecules* **2005**, *38*, 1099−1106.
(21) Konn, C.; Morel, F.; Beyou, E.; Chaumont, P.; Bourgeat-Lami, E. *Macromolecules* **2007**, *40*, 7464−7472.
(22) Hawker, C. J.; Barclay, G. G.; Orellana, A.; Dao, J.; Devonport, W. *Macromolecules* **1996**, *29*, 5245−5254.
(23) Hawker, C. J.; Bosman, A. W.; Harth, E. *Chem. Rev.* **2001**, *101*, 3661−3688.
(24) Kuwabara, Y.; Ogawa, H.; Inada, H.; Noma, N.; Shirota, Y. *Adv. Mater.* **1994**, *6*, 677−679.
(25) Yasuda, T.; Shinohara, Y.; Matsuda, T.; Han, L.; Ishi-i, T. *J. Mater. Chem.* **2012**, *22*, 2539−2544.
(26) Bach, U.; Lupo, D.; Comte, P.; Moser, J. E.; Weissortel, F.; Salbeck, J.; Spreitzer, H.; Gratzel, M. *Nature* **1998**, *395*, 583−585.
(27) Hsu, C. Y.; Chen, Y. C.; Lin, R. Y. Y.; Ho, K. C.; Lin, J. T. *Phys. Chem. Chem. Phys.* **2012**, *14*, 14099−14109.
(28) Burschka, J.; Dualeh, A.; Kessler, F.; Baranoff, E.; Cevey-Ha, N. L.; Yi, C. Y.; Nazeeruddin, M. K.; Gratzel, M. *J. Am. Chem. Soc.* **2011**, *133*, 18042−18045.
(29) Snaith, H. J.; Humphry-Baker, R.; Chen, P.; Cesar, I.; Zakeeruddin, S. M.; Gratzel, M. *Nanotechnology* **2008**, *19*, 424003.
(30) Chung, I.; Lee, B.; He, J. Q.; Chang, R. P. H.; Kanatzidis, M. G. *Nature* **2012**, *485*, 486−U494.
(31) Lee, M. M.; Teuscher, J.; Miyasaka, T.; Murakami, T. N.; Snaith, H. J. *Science* **2012**, *338*, 643−647.
(32) Xia, H. J.; He, J. T.; Xu, B.; Wen, S. P.; Li, Y. W.; Tian, W. J. *Tetrahedron* **2008**, *64*, 7837−7838.
(33) Grimaldi, S.; Finet, J. P.; Le Moigne, F.; Zeghdaoui, A.; Tordo, P.; Benoit, D.; Fontanille, M.; Gnanou, Y. *Macromolecules* **2000**, *33*, 1141−1147.
(34) Bailly, B.; Donnenwirth, A. C.; Bartholome, C.; Beyou, E.; Bourgeat-Lami, E. *J. Nanomater.* **2006**, DOI: Sp Issue, 76371, DOI: 10.1155/JNM/2006/76371.
(35) Laruelle, G.; Parvole, J.; Francois, J.; Billon, L. *Polymer* **2004**, *45*, 5013−5020.
(36) Ding, I. K.; Tetreault, N.; Brillet, J.; Hardin, B. E.; Smith, E. H.; Rosenthal, S. J.; Sauvage, F.; Gratzel, M.; McGehee, M. D. *Adv Funct Mater* **2009**, *19*, 2431−2436.
(37) Kim, H. S.; Lee, C. R.; Jang, I. H.; Kang, W.; Park, N. G. *Bull. Korean Chem. Soc.* **2012**, *33*, 670−674.
(38) Wang, X.; Zhi, L. J.; Mullen, K. *Nano Lett* **2008**, *8*, 323−327.
(39) Barea, E. M.; Garcia-Belmonte, G.; Sommer, M.; Huttner, S.; Bolink, H. J.; Thelakkat, M. *Thin Solid Films* **2010**, *518*, 3351−3354.
(40) Poplavskyy, D.; Nelson, J. *J. Appl. Phys.* **2003**, *93*, 341−346.
(41) Cappel, U. B.; Daeneke, T.; Bach, U. *Nano Lett* **2012**, *12*, 4925−4931.
(42) Zaban, A.; Greenshtein, M.; Bisquert, J. *Chemphyschem* **2003**, *4*, 859−864.
(43) Haque, S. A.; Tachibana, Y.; Willis, R. L.; Moser, J. E.; Gratzel, M.; Klug, D. R.; Durrant, J. R. *J Phys Chem B* **2000**, *104*, 538−547.
(44) Haque, S. A.; Palomares, E.; Cho, B. M.; Green, A. N. M.; Hirata, N.; Klug, D. R.; Durrant, J. R. *J. Am. Chem. Soc.* **2005**, *127*, 3456−3462.